

EXPERIMENTAL STUDY AND MODELING OF PRE-DEFORMATION EFFECT ON AUSTENITE TO FERRITE TRANSFORMATION

A.A. Vasilyev^{1*}, D.F. Sokolov², S.F. Sokolov², A.A. Zisman¹

¹Peter the Great St. Petersburg Polytechnic University, Polytekhnicheskaya, 29, 195251, St. Petersburg, Russia

²PJSC Severstal, Mira, 30, 162608, Cherepovets, Russia

*e-mail: vasilyev_aa@mail.ru

Abstract. Transformation kinetics of undeformed and deformed austenite during continuous cooling has been investigated on several industrial steels. Dimensions of both prior austenite grains and ferrite grains in ferrite-pearlite structures obtained for various states of parent austenite and cooling rates were determined. Based on the obtained experimental data a physically motivated model is formulated for the ferritic transformation with allowance for the effects of deformation and concurrent recovery of austenite. Under consideration is the deformation influence on both the nucleation and growth of the ferrite grains. The model is first to evaluate the variation of nucleation barriers owing to the hydrostatic component of internal stresses at austenite grain boundaries. The modeling results significantly dependent on this issue comply well with experimental data on the kinetics of ferritic-pearlitic transformation and final ferrite grain size in the considered steels.

Keywords: steels, austenite, deformation, recovery, transformation, ferrite, modeling

1. Introduction

Finish stages of industrial hot rolling of microalloyed HSLA steels are often implemented at appropriately low temperatures so that deformation-induced precipitation of carbo-nitrides hinders the austenite recrystallization [1]. Thus, retained strain accumulates that affects fractions and morphologies of specific structural constituents produced by the phase transformation in subsequent accelerated cooling as well as the final mechanical properties of steel. Related quantitative models should allow for the austenite deformation effect on the formation of all transformation products including ferrite. Although the latter is not the main structural component of high strength steels, its appearance in the initial transformation stage significantly influences the following formation of bainite that essentially determines the material properties [2].

There are several works [3-8] devoted to experimental study and modeling of the pre-deformation effect on the austenite to ferrite transformation in continuous cooling. It is accepted that this effect accelerates the transformation as displayed by the increase of its start and finish temperatures. It is also accepted as well that deformation leads to a certain reduction in ferrite grain size. Literature data on the considered effect are surveyed in [6] that also formulates the model allowing for the accelerating influence of austenite deformation on the ferrite growth rate in plain carbon steel. The nucleation kinetics as such was not analyzed in this work. Instead, ferrite embryos were assumed to appear at austenite grain boundaries as soon as certain overcooling is reached. The density of the embryos was evaluated in terms of measured grain size in the transformed structures. An important result of this study is that the main factor accelerating the transformation is a reduction of the required overcooling rather

than the increased growth rate or a change in the nucleation site density. It is worth noting as well that the diminished characteristic overcooling is hardly due to higher dislocation density in deformed austenite since the respective increase in its specific energy is insufficient.

According to [9,10], the rate of any nucleation process exponentially increases with a variation of corresponding energy barriers around their average value. The authors believe that such variations may appear in the deformed austenite as far as interaction of its constitutive grains results in strong residual stress singularities at grain ribs [11] and hence apexes. Owing to a volumetric effect of the $\gamma \rightarrow \alpha$ transformation in steel, hydrostatic components of the internal stresses will affect the nucleation whereas alternate signs of them naturally comply with the general "static disorder" concept [9,10]. Specifically, in comparison to undeformed austenite, the transformation starts at lesser overcooling because of positive (tensile) hydrostatic stresses in some local domains although the process is delayed in other local domains where the hydrostatic component is negative. The present paper is first to model the considered effect and to verify it.

In this work, the experimental study of the austenite transformation leading to ferrite-pearlite structures is performed on several industrial steels with and without the austenite pre-deformation. Based on the obtained results and additional measurements of ferrite grain sizes, a physically motivated model is formulated for the ferrite transformation with allowance for the effects of deformation and concurrent recovery of austenite.

2. Materials and experimental methods

Chemical compositions of seven investigated steels produced at PJSC Severstal are shown in Table 1. To analyze the effect of pre-deformation on austenite transformation under continuous cooling, the Pocket Jaw unit of thermomechanical simulator Gleeble 3800 has been applied according to a scheme in Fig. 1a. After cooling to temperature T_d test samples are held for 5 s (or compressed with strain rate 1 s^{-1} to true strain $\varepsilon = 0.4$ and held for 5 s), and cooled with various rates (1, 3, 10, 30 и 100°C/s) to room temperature. Austenitizing temperatures T_a (Table 2) are selected so that holding time $t_a = 60 \text{ s}$ would not lead to excessive grain growth. To avoid deformation-induced ferrite transformation [12], deformation temperatures T_d are above A_3^{PE} corresponding to para-equilibrium of ferrite and austenite according to Thermo-Calc calculations [13]. No transformation during the deformation of austenite has been verified by dilatometry data. Besides, with a slow cooling (1°C/s) in the ferrite temperature range (Fig. 1b), thin ferrite layers along prior austenite grain boundaries (PAGB) have been formed and then revealed by etching in a 3% water solution of picric acid at 80°C . Quenching temperatures T_q were selected to get a ferrite volume fraction of about 10%. The ferrite-pearlite microstructures have been revealed using Nital reactive at room temperature. Planar sections were prepared by standard metallographic procedures and then investigated on optical microscope Axio Observer "Carl Zeiss" equipped with a computerized image analysis system. Presuming equiaxed shapes of both PAG and ferrite grains, respective average volumetric diameters D_γ and D_α have been derived from their planar counterparts.

Table 1. Chemical compositions (mass.%) of the investigated steels

Steels	C	Mn	Si	Cr	Ni	Mo	Nb	V	Ti
S1	0.06	0.17	0.01	0.02	0.03	0.004	0.002	0.002	0.001
S2	0.13	0.40	0.02	0.04	0.04	0.004	0.002	0.002	0.001
S3	0.18	0.70	0.20	0.03	0.05	0.003	0.002	0.010	0.001
S4	0.20	0.40	0.19	0.03	0.03	0.004	0.002	0.004	0.002
S5	0.11	1.55	0.66	0.03	0.03	0.003	0.003	0.005	0.003
S6	0.23	1.31	0.05	0.03	0.03	0.007	0.003	0.005	0.003
S7	0.10	0.56	0.55	0.21	0.25	0.120	0.022	0.065	0.004

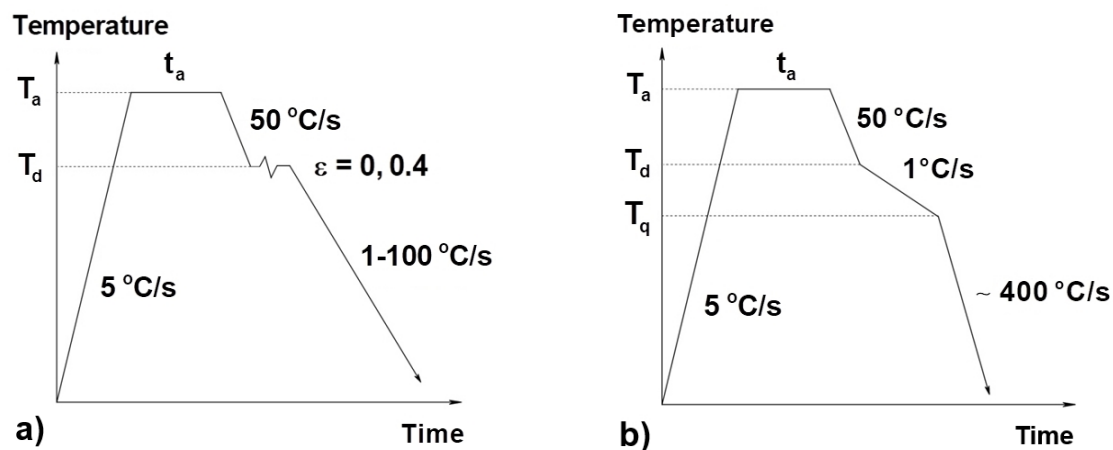


Fig. 1. Schemes of experiments on Gleeble 3800 to investigate the phase transformation of undeformed and deformed austenite under different cooling conditions (a) and to form ferrite layers along PAGB (b)

Table 2. Characteristic temperatures of steel treatments and respective average diameters of PAG

Steels	T_a , °C	A_3^{PE} , °C	T_d , °C	T_q , °C	D_γ , μm
S1	1000	878	900	880	35
S2	950	838	900	798	55
S3	950	817	950	770	20
S4	950	824	900	802	24
S5	1000	811	850	765	22
S6	950	778	850	720	29
S7	1200	858	900	820	131

3. Experimental results

Two examples of microstructures used to determine PAG sizes are shown in Fig. 2. According to Table 2, these sizes vary in a wide range of 20 to 131 μm . Among 35 couples of transformed microstructures (7 steels and 5 cooling rates) corresponding to both undeformed and deformed austenite, the present work considers only 24 couples of ferrite-pearlite structures. Most of them were obtained at cooling rates 1, 3, and 10 °C/s. For steels S1, S2, and S4 structures of this type were also obtained at a rate 30 °C/s (Fig. 3).

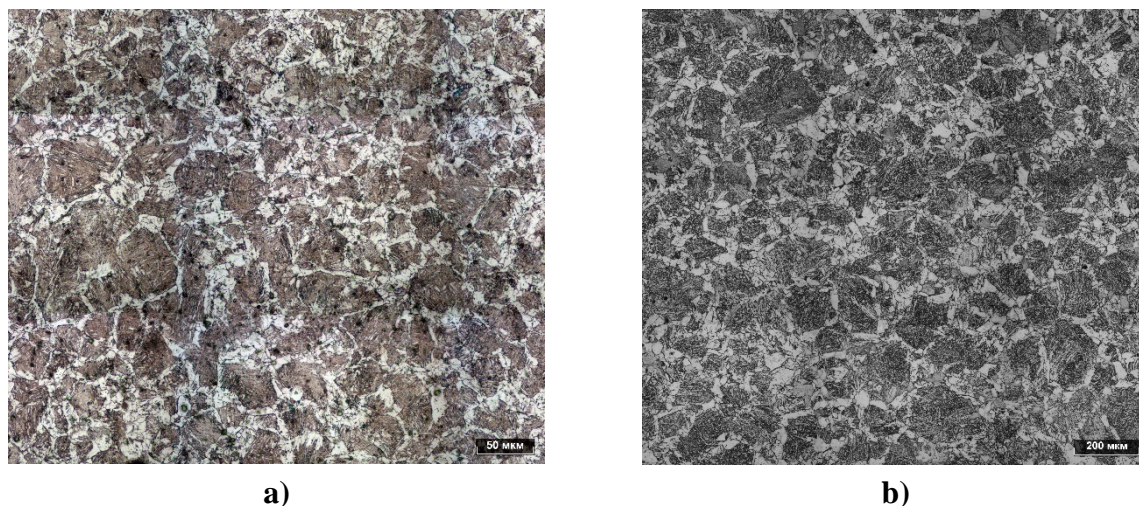
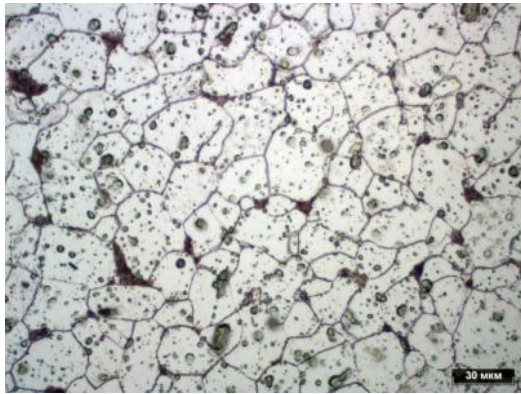


Fig. 2. Microstructures of steels S1 (a) and S7 (b) used to quantify dimensions of PAGB

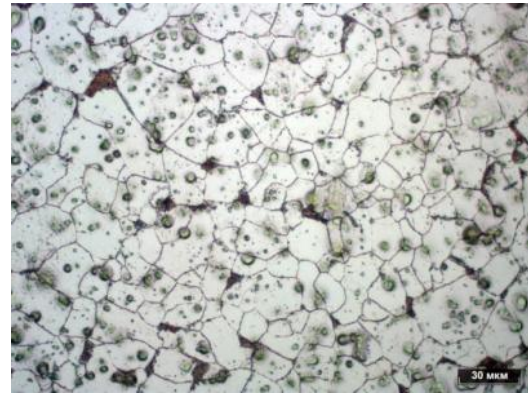
According to Figs. 4a,c,e, at low cooling rates (1 and 3°C/s) there is no notable effect of austenite deformation on the start temperature T_S of ferritic transformation. At the same time, the deformation effect gains in significance at higher cooling rates that is seemingly due to weaker recovery of the deformed austenite structure. Similarly, the austenite deformation influences the temperature T_F of the transformation finish although in this case, the cooling rate effect on the increase of this temperature is lesser. In all, as expected, the pre-deformation of austenite shifts the transformation range to higher temperatures.

According to obtained results, the transformation of deformed austenite generally leads to finer ferrite grains. This effect is confirmed by structures of steels S1, S5 and S6 obtained at a cooling rate 3°C/s (Fig. 3), as well as by Figs. 4b,f. However, in some cases (8 couples of structures) ferrite grains appearing from deformed austenite at low cooling rates (1 and 3°C/s) proved to be coarser with respect to no deformation (see e.g. Fig. 4d). It is worth noting that such deviations are close to the measurement error of about at least 1 μm. Possible reasons for such exclusion will be further discussed in section 4.

When averaged over all analyzed structures, the refinement of ferrite grains due to austenite deformation becomes notable with increasing cooling rate but remains rather weak. Thus, average grain sizes corresponding to 1, 3, and 10°C/s are 15.5, 12.2, and 10.3 μm reduced by only 2, 3 и 10% to no deformation case. Even at the most cooling rate of 10°C/s the apparent refinement is comparable to the measurement error. The maximum relative reduction of grain size reaches about 20% in steels S1, S2, and S6.

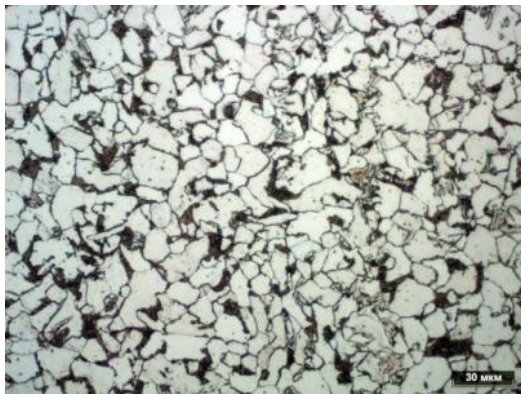


$$D_{\alpha} = 18.0 \mu\text{m}$$

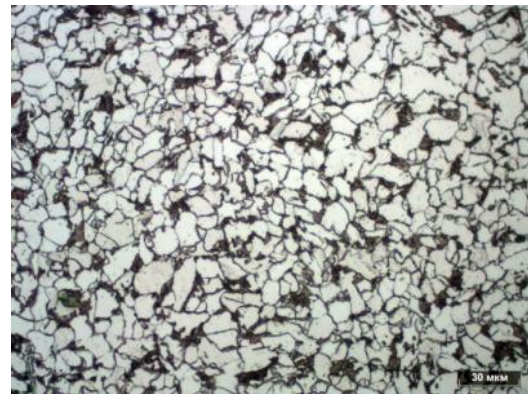


$$D_{\alpha} = 15.7 \mu\text{m}$$

a)



$$D_{\alpha} = 9.5 \mu\text{m}$$



$$D_{\alpha} = 7.4 \mu\text{m}$$

b)



$$D_{\alpha} = 7.4 \mu\text{m}$$



$$D_{\alpha} = 7.1 \mu\text{m}$$

c)

Fig. 3. Ferrite-perlite microstructures (average grain diameters indicated) due to the transformation of undeformed (left) and deformed (right) austenite at a cooling rate $3^{\circ}\text{C}/\text{s}$. Structures (a), (b), and (c) correspond to steels S1, S5 and S6, respectively

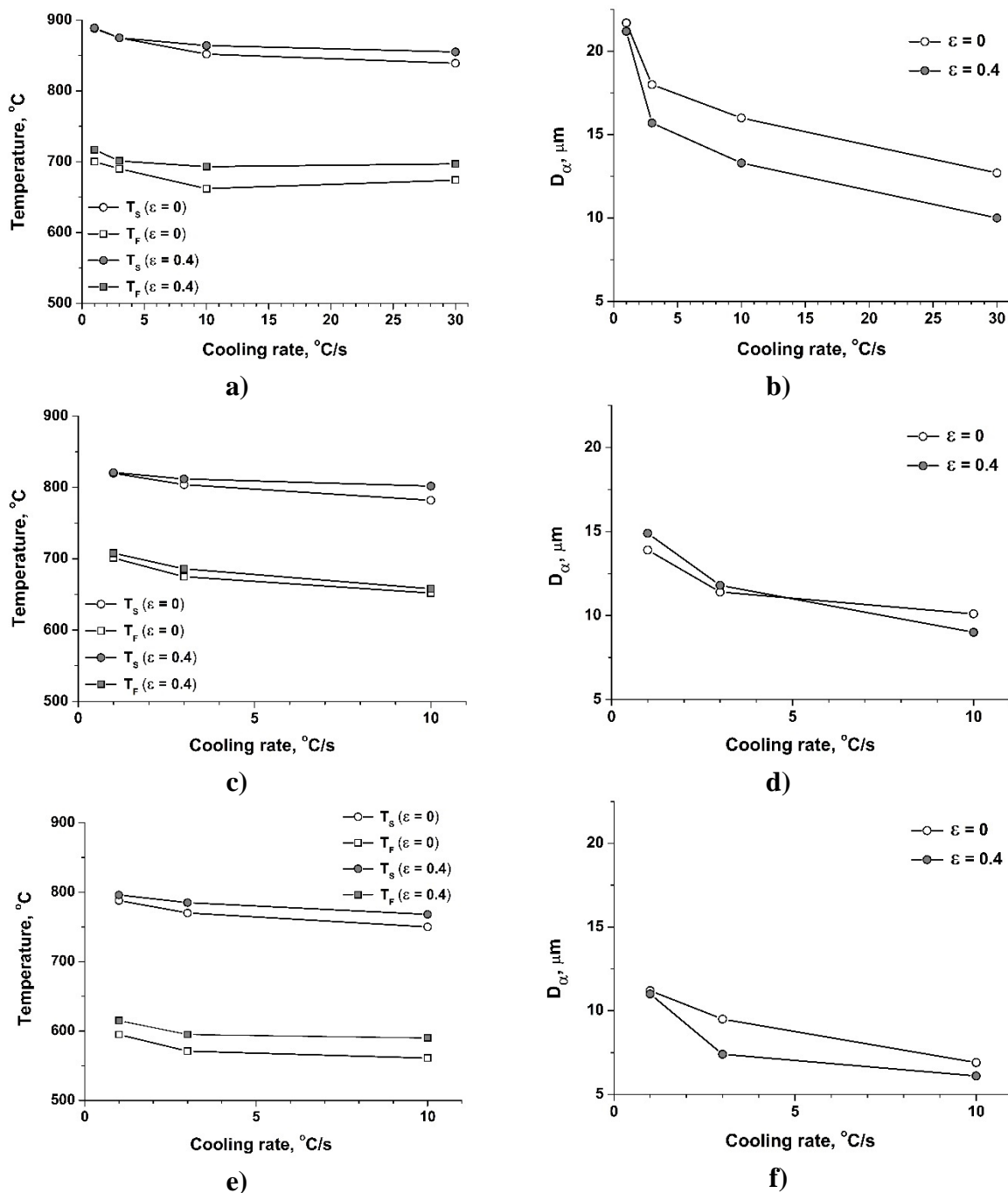


Fig. 4. Dependences of the start (T_s) and finish (T_f) temperatures of austenite transformation (left) and of ferrite grain size (right) on the cooling rate for steels S1 (a,b), S4 (c,d), and S5 (e,f)

4. Model description

The above-considered experimental data have been employed to calibrate the present model that is an extension of the previous one [14] where the austenite deformation effect was not considered.

Ferrite nucleation. Regardless of austenite state (undeformed or deformed), polygonal ferrite is presumed to nucleate at PAGB in two modes. In the first mode, the nucleation sites are apexes of austenite grains, in the second one linear junctions (ribs) of them serve as ferrite

origins. On considering 5 apexes per grain and allowing their gradual occupation in time, the volume density $N_1^0(t)$ of related nucleation sites takes on form [14]:

$$N_1^0(t) \cong \frac{10}{D_\gamma^3} - \Delta N_1(t), \quad (1)$$

where D_γ is the average diameter of austenite grains and $\Delta N_1(t)$ is the density of ferrite grains nucleated in time t calculated from the moment when ferrite formation becomes thermodynamically favorable.

In the second mode, the ferrite nucleation at ribs of austenite grains is considered. The ferrite propagation along ribs and facets is treated so that the current density of related nucleation sites is expressed by [14]:

$$N_2^0(t) = \frac{1}{D_\gamma^2 a_\gamma} (1 - S_\alpha(t)), \quad (2)$$

where a_γ is the austenite lattice parameter and $S_\alpha(t)$ is the PAGB fraction occupied by ferrite at time t .

Since the ferrite nucleation is a thermo-activated lattice rearrangement, the austenite deformation effect on the considered modes ($k = 1, 2$) at current time t at absolute temperature T is revealed in terms of the classical nucleation theory [14] modified as proposed in [9]. The resulting nucleation rate is:

$$J_k(T, Y_{AE}, \varepsilon, t, t_C) = C_k N_k^0(t) \exp\left(-\frac{Q_N(Y_{AE})}{R_g T}\right) \exp\left(-\frac{\Psi_k^{PF}(\varepsilon, t_C) \sigma_k^3}{k_B T \Delta G_{\gamma \rightarrow \alpha}^2(T, Y_{AE}, \varepsilon, t_C)}\right). \quad (3)$$

In this expression $Q_N(Y_{AE})$ is the activation energy of the lattice rearrangement, $Y_{AE} = \{y_C, y_{Mn}, y_{Si}, \dots\}$ represents a set of average fractions of the sites of substitution and interstitial sublattices occupied, respectively, by the atoms of substitution alloying elements and carbon. Parameter σ_k expresses effective specific energy of γ/α - interface, $\Delta G_{\gamma \rightarrow \alpha}(T, Y_{AE}, \varepsilon, t_C)$ is the transformation driving force dependent on strain degree ε of austenite, time t_C is counted from the end of deformation, the factor $\Psi_k^{PF}(\varepsilon, t_C)$ is equal to unity in case of no pre-deformation and allows for variation of nucleation barriers in deformed austenite due to alternate signs of internal hydrostatic stresses at morphological features of grain boundaries [11]. Boltzmann's constant and the universal gas constant are conventionally denoted by k_B and R_g .

The driving force of austenite transformation

$$\Delta G_{\gamma \rightarrow \alpha}(T, Y_{AE}, \varepsilon, t_C) = \Delta G_{\gamma \rightarrow \alpha}^0(T, Y_{AE}) + \Delta G_{\gamma \rightarrow \alpha}^d(\varepsilon, t_C) \quad (4)$$

involves both term $\Delta G_{\gamma \rightarrow \alpha}^0(T, Y_{AE})$ peculiar to undeformed austenite and specific contribution of deformation

$$\Delta G_{\gamma \rightarrow \alpha}^d(\varepsilon, t_C) \cong -0.5b^2 \mu \bar{\rho}_d(\varepsilon, t_C), \quad (5)$$

where b is the Burgers vector magnitude, μ is the shear modulus, and $\bar{\rho}_d(\varepsilon, t_C)$ is the average dislocation density. Based on the general expression for the dislocation part of work hardening and allowing for recovery (see Eqs. (10)-(11)), we employ:

$$\bar{\rho}_d(\varepsilon, t_C) = \left(\frac{\Delta \sigma(\varepsilon, t_C)}{\alpha_p M \mu b} \right)^2, \quad (6)$$

where $M = 3.1$ is the Taylor factor and $\alpha_p \cong 0.15$. The temperature dependence of μ is evaluated according to [15]:

$$\mu \equiv \mu(T) = 8.1 \times 10^{10} \left(0.91 - \frac{T - 300}{1810} \right) (Pa). \quad (7)$$

The factor ψ_k^{PF} is evaluated according to [9]:

$$\psi_k^{PF} = (1 + 3\xi_k + \xi_k^2)(1 + \xi_k)^{-3}, \quad (8)$$

where ξ_k is proportional to the driving force variation due to hydrostatic stresses induced in the interaction of deformed austenite grains. With allowance for the relative volume change $\delta_{\gamma \rightarrow \alpha}$ in $\gamma \rightarrow \alpha$ transformation, we will consider the driving force dispersion proportional to $(\delta_{\gamma \rightarrow \alpha} \Delta\sigma(\varepsilon, t_C))^2$ and thus obtain [9]:

$$\xi_k \equiv \xi_k(t_C) = \alpha_{\xi_k} \frac{\alpha_{\gamma}^4 (\delta_{\gamma \rightarrow \alpha} \Delta\sigma(\varepsilon, t_C))^2}{\sigma_k k_B T}, \quad (9)$$

where α_{ξ_k} are empirical coefficients ($k = 1, 2$). Note that at $\xi_k > 0$ parameters $\psi_k^{PF} < 1$ and monotonously diminishes with growing ξ_k . Hence, the higher dispersion of driving force proportional to $(\delta_{\gamma \rightarrow \alpha} \Delta\sigma(\varepsilon, t_C))^2$, the lesser an effective barrier value in Eq. (3) providing an exponential increase of the nucleation rate.

The weakening of work hardening through recovery is expressed according to [16]:

$$\frac{d\Delta\sigma(\varepsilon, t_C)}{dt} = -\frac{64\Delta\sigma(\varepsilon, t_C)^2 v_d}{9M^3 \alpha_p^2 E(T)} \exp\left(-\frac{U_{rec}}{R_g T}\right) \sinh\left(\frac{\Delta\sigma(\varepsilon, t_C) V_{rec}}{k_B T}\right), \quad (10)$$

where U_{rec} and V_{rec} , respectively, are activation energy and activation volume of the recovery process that are assumed to be equal 286 kJ/mol and $45b^3$ [17]; v_d is the Debye frequency set to be $2 \times 10^{12} \text{ s}^{-1}$, $E(T) = 2.6\mu(T)$ is Young's modulus. To integrate Eq. (10), the initial condition

$$\Delta\sigma(\varepsilon, t_C = 0) = \sigma_\varepsilon - \sigma_y \quad (11)$$

is used, where σ_ε is the deforming stress of austenite, dependent on strain degree, strain rate, and temperature according to [17], and $\sigma_y \equiv \sigma_{0.2}$ is the yield stress of austenite similarly calculated at its plastic strain of 0.2%.

We consider activation energy Q_N of the diffusional lattice rearrangement equal to that of the grain boundary self-diffusion estimated as half of the activation energy Q_{SD} of the bulk self-diffusion. Thus, to simplify the modeling, the known dependence of Q_{SD} on chemical composition Y_{AE} according to [18]

$$\begin{aligned} Q_{SD}(Y_{AE}) = & 311691 - 278242(1 - \exp(-0.394y_C)) + 88752y_{Mn}^{0.31} + 22801y_{Si} - \\ & - 6490y_{Cr} + 84864y_{Mo}^{0.65} - 38575y_{Ni}^{0.3} - 7298y_V + 132594y_{Nb}^{0.263} + \\ & + 82128y_{Ti}^{0.401} (J/mol) \end{aligned} \quad (12)$$

can be utilized by $Q_N(Y_{AE}) = 0.5Q_{SD}(Y_{AE})$.

Ferrite growth. The ferrite growth rate is treated in terms of the "mixed kinetics" [19] where the movement of γ/α - interface is controlled by both its mobility and the rate of carbon displacement from the interface to the volume of austenite grain. The growth rate in the general case is determined by the most hindering factor of the two.

The velocity of moving γ/α – interface (ferrite growth rate) where the lattice rearrangement takes place is expressed according to [14]:

$$V_{\gamma/\alpha}^L(T, Y_{AE}^*, \varepsilon, t_C) = -M_{\gamma/\alpha}(T, Y_{AE}^*) \Delta G_{\gamma \rightarrow \alpha}(T, Y_{AE}, \varepsilon, t_C)$$

$$M_{\gamma/\alpha}(T, Y_{AE}^*) = M_{\gamma/\alpha}^0 \exp\left(-\frac{Q_G(Y_{AE}^*)}{R_g T}\right), \quad (13)$$

where $M_{\gamma/\alpha}(T, Y_{AE}^*)$ is the mobility of the interphase boundary, $Q_G(Y_{AE}^*)$ is the effective activation energy of the lattice rearrangement, and $M_{\gamma/\alpha}^0$ is an empirical parameter. The term Y_{AE}^* differs from Y_{AE} by the carbon content; the former contains y_C^* (effective concentration of carbon in the moving γ/α – interface) whereas in the latter the carbon concentration y_C is equal to its average value in austenite. Following [14], the activation energy of growth is evaluated by $Q_G(Y_{AE}^*) = 0.5Q_{SD}(Y_{AE}^*)$, where y_C^* is the average value between y_{C_α} and $y_{C_\gamma}^{\text{int}}$, y_{C_α} is equilibrium (para-equilibrium) carbon concentration in ferrite and $y_{C_\gamma}^{\text{int}}$ is its interfacial concentration on the austenite side.

To simplify the self-consistent calculations of the carbon effective interfacial concentration the transformation driving force in (12) is expressed by [19]:

$$\Delta G_{\gamma \rightarrow \alpha}(T, Y_{AE}, \varepsilon, t_C) \approx \alpha_G(x_{C_\gamma}^{\text{int}} - x_{C_\gamma}) + \Delta G_{\gamma \rightarrow \alpha}^d(\varepsilon, t_C), \quad (14)$$

where x_{C_γ} and $x_{C_\gamma}^{\text{int}}$ are, respectively, equilibrium (para-equilibrium) and interfacial carbon molar fractions (relation between site and molar fractions of carbon is given by: $y_C = x_C / (1 - x_C)$) and $\alpha_G > 0$ is an empirical coefficient. When evaluating the rate of ferrite growth, controlled by the carbon displacement from a moving interphase boundary, an approximation of spherical grain is used:

$$V_{\gamma/\alpha}^C(T, Y_{AE}) = \frac{\bar{D}_C(T, Y_{AE}) (x_{C_\gamma}^{\text{int}} - x_C)}{R_\alpha (x_{C_\gamma}^{\text{int}} - x_{C_\alpha})}, \quad (15)$$

where $\bar{D}_C(T, Y_{AE})$ is the bulk diffusion coefficient of carbon in austenite averaged in the range $[x_C; x_{C_\gamma}^{\text{int}}]$, R_α is the grain radius. The effects of alloying on this diffusion coefficient have been allowed for according to [20]. Effective interface concentration $x_{C_\gamma}^{\text{int}}$ varying in the range $[x_C; x_{C_\gamma}]$ is found by numerical solution of transcendental equation:

$$\frac{\bar{D}_C(T, Y_{AE}) (x_{C_\gamma}^{\text{int}} - x_C)}{R_\alpha (x_{C_\gamma}^{\text{int}} - x_{C_\alpha})} = -M_{\gamma/\alpha}(T, Y_{AE}^*) (\alpha_G (x_{C_\gamma}^{\text{int}} - x_{C_\gamma}) + \Delta G_{\gamma \rightarrow \alpha}^d(\varepsilon, t_C)). \quad (16)$$

Then, with obtained $x_{C_\gamma}^{\text{int}}$, the rate of ferrite grain growth is calculated using (15).

Additional components of the model. Following [14], volume increments dv_1 and dv_2 of ferrite grains nucleated in the first and second modes, respectively, are calculated with allowance for the grain "hard collisions". The ferrite nucleation is completed at the time t_N , where this phase covers all the area of austenite boundaries: $S_\alpha(t_N) = 1$. Next, rapid increments dS_α along austenite boundaries are also determined according to [14]. Besides, this paper describes the calculation of employed thermodynamic parameters (driving force $\Delta G_{\gamma \rightarrow \alpha}^0(T, Y_{AE})$ of transformation of undeformed austenite and equilibrium carbon

concentrations ($y_{C_\gamma}, y_{C_\alpha}$ in both phases) dependent on temperature and chemical composition.

The average volumetric diameter of ferrite grains that is an important characteristic of ferrite-pearlite structures is expressed according to [21]:

$$D_\alpha = 1.5 \times \left(\frac{2X_\alpha}{3N_\alpha} \right)^{1/3}, \quad (17)$$

where X_α is the volume fraction of ferrite, $N_\alpha = N_1(t_N) + N_2(t_N)$ is the number of grains per unit volume. A model used for the pearlitic transformation is described in [14] as well.

5. Model calibration, modeling results, and their discussion

Empirical parameters of the present model have been determined in [14], except for α_{ξ_1} and α_{ξ_2} reflecting the accelerating effect of austenite deformation. The latter two parameters are found with allowance for an accumulated database on the transformation kinetics of deformed austenite in the considered steels as well as on ferrite grain sizes in corresponding structures. A set of the considered parameters is optimized to minimize the difference between the model and experimental curves for the transformation kinetics as well as between the predicted and measured sizes of ferrite grains. The problem is solved with allowance for 24 kinetic curves and corresponding data on the grain sizes. The calculations have been implemented with the authors' model/software AusEvol Pro [22] that enables quantification of microstructure evolution both during hot deformation of austenite and during its transformation in cooling where main structural constituents (ferrite, perlite, bainite, and martensite) are specifically allowed for. The previous version [14] of this model has been modified to simulate the ferrite transformation with allowance for the austenite deformation effect.

Input $a_\gamma = 0.364$ nm, $\delta_{\gamma \rightarrow \alpha} = 0.02$, $\sigma_1 = 0.016$ and $\sigma_2 = 0.028$ J/m² [14] (see Eq. (9)) have resulted in $\alpha_{\xi_1} = 1.82 \times 10^3$, $\alpha_{\xi_2} = 2.92 \times 10^3$. Other conditions being equal, these results mean that the nucleation rate of ferrite grains in the second mode (at ribs of grains) increases stronger concerning the first mode (at grain apexes). This complies with the appearance of local hydrostatic stresses in deformed austenite just at grain ribs [11] whereas stresses around grain apexes want further analysis.

Figure 5 enables a comparison of calculated kinetics of the ferritic-pearlitic transformation to respective experimental data for several investigated steels. The modeling results comply satisfactorily with experiments. Experimental verification of predicted ferrite grain sizes obtained from both undeformed and deformed austenite is satisfactory as well (Fig. 6). Relative errors of these predictions averaged over all considered steels are, respectively, 10.8 and 13.2%.

It is worth noting that the simulated refinement of ferrite grains due to the pre-deformation of austenite is rather modest. Moreover, predicted grain sizes corresponding to relevant experiments sometimes exceed those in the case of undeformed austenite. A plausible explanation of such results is that the pre-deformation may both increase the number of embryonic grains and accelerate their growth because of higher transformation temperatures. Accordingly, the number of available nucleation sites for the second mode (see Eq. (2)) is faster exhausted that leads to coarser final grains.

Figure 7 displays TTT diagrams of austenite transformation in steel DP-600 (0.08C, 1.7Mn, 0.2Cr, 0.2Mo) calculated with program AusEvol Pro [22] for both deformed (true strain 0.4, strain rate 1 s⁻¹) and undeformed states at the PAG size of 50 μ m. At the cooling mode shown in this figure, final structure parameters predicted with and without the austenite deformation are listed in Table 3. Apparently, in the considered case the deformation effect on

the transformation significantly change both the steel structure and mechanical properties. According to these results, an integral model of austenite transformation undoubtedly should allow for the austenite pre-deformation.

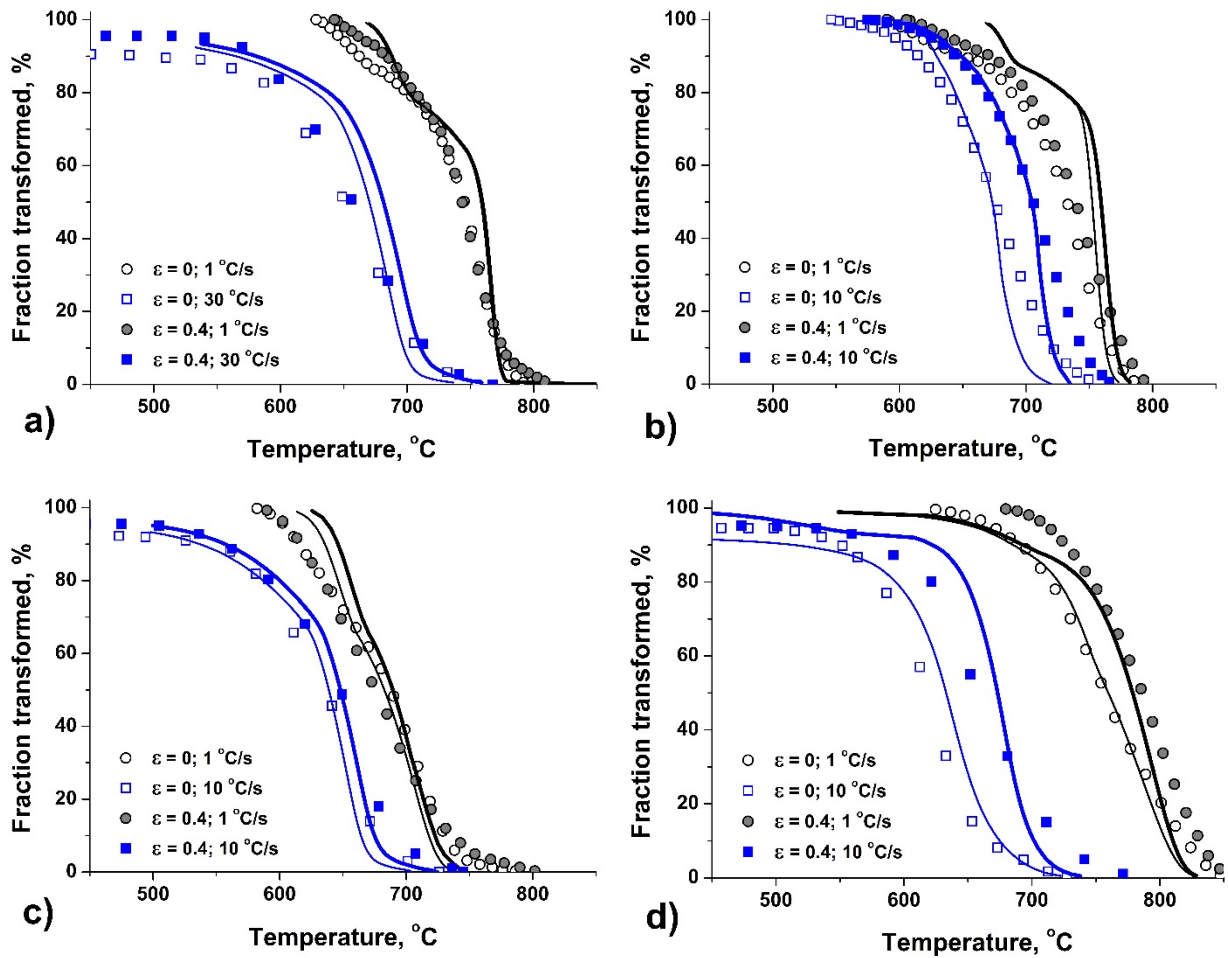


Fig. 5. Austenite transformation kinetics by the model (lines) and experiments (symbols) for steels S3 (a), S5 (b), S6 (c), and S7 (d)

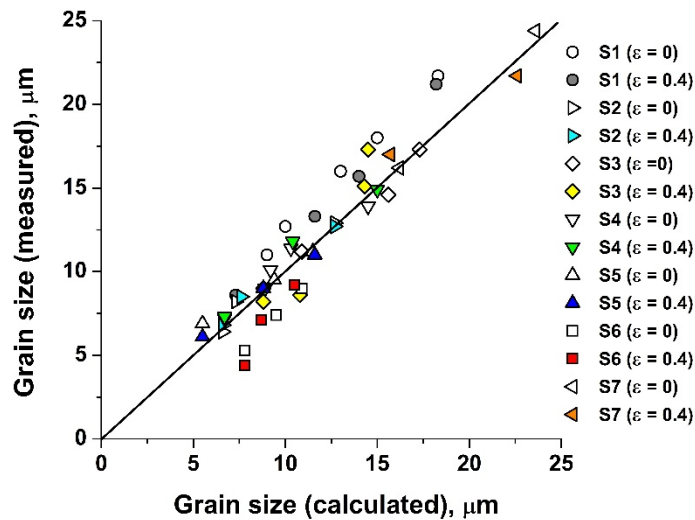


Fig. 6. Comparison of calculated and measured ferrite grain sizes for investigated steels and strain degrees

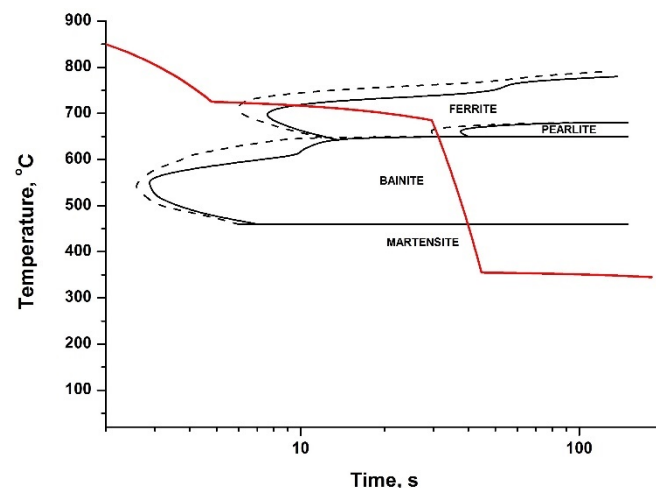


Fig. 7. TTT diagrams of austenite transformation from undeformed (solid lines) and deformed (dashed lines) states of the considered steel. A red line represents the cooling mode

Table 3. Microstructure parameters and mechanical properties calculated regardless of austenite deformation ($\varepsilon = 0$) and with allowance for the latter

	Volume fraction			Ferrite grain size, μm	Yield stress, MPa	Tensile stress, MPa	Elongation (A5), %
	Ferrite	Pearlite	Martensite				
$\varepsilon = 0$	0.88	0.01	0.11	8.0	611	677	28
$\varepsilon = 0.4$	0.96	0.02	0.02	6.8	397	466	32

6. Conclusions

Transformation kinetics of both undeformed and deformed (true strain 0.4) austenite have been investigated with the Pocket Jaw unit of thermomechanical simulator Gleeble 3800 for seven industrial steels at various rates of continuous cooling (1, 3, 10, 30, and 100°C/s). Besides, to evaluate the deformation effect, sizes of ferrite grains and PAG have been determined for 24 couples (undeformed/deformed austenite) of ferrite-pearlite structures at various cooling rates and parent austenite states. It is shown that the pre-deformation generally elevates the transformation start temperature. This effect is not notable at low cooling rates but gains in significance for the higher rates due to weaker recovery of the deformed austenite structure. In all, austenite deformation shifts the transformation range to higher temperatures.

When averaged over all analyzed structures, refinement of ferrite grains due to austenite deformation becomes more notable with increasing cooling rates but remains rather weak. Thus, average grain sizes corresponding to 1, 3, and 10°C/s are reduced only by 2, 3, and 10% to no deformation case. Even at the most cooling rate of 10°C/s an apparent decrease in grain size is comparable to the measurement error.

Based on the obtained experimental data, a physically motivated model is formulated for the ferrite transformation with allowance for the effects of deformation and concurrent recovery of austenite on both the nucleation and growth of ferrite grains. To predict properly the nucleation rate, the variation of nucleation barriers at austenite grain boundaries is considered which is due to the hydrostatic component of deformation-induced internal stresses. The present model is first to allow for this effect exponentially increasing the nucleation rate. Simulated kinetics of the ferritic-pearlitic transformation in the investigated steels satisfactorily comply with experiments. Experimental verification of ferrite grain sizes predicted for both undeformed and deformed austenite is satisfactory as well. Relative errors of these predictions averaged over all considered steels are 10.8 and 13.2%, respectively.

Acknowledgments. This work was supported by the grant from the Russian Science Foundation (project No. 19-19-00281).

References

- [1] Militzer M. Thermomechanical processed steels. In: Hashmi S, Van Tyne CJ. (eds.) *Comprehensive Materials Processing. V.1. Assessing Properties of Conventional and Specialized Materials*. 2014. p.191-216.
- [2] Ravi AM, Kumar A, Herbig M, Sietsma J, Santofimia MJ. Impact of austenite grain boundaries and ferrite nucleation on bainite formation in steels. *Acta Materialia*. 2020;188: 424-434.
- [3] Essadiqi E, Jonas JJ. Effect of deformation on the austenite-to-ferrite transformation in a plain carbon and two microalloyed steels. *Metallurgical Transactions A*. 1988;19: 417-426.
- [4] Umamoto M, Hiramatsu A, Moriya A, Watanabe T, Nanba S, Nakajima N, Anan G, Higo Y. Computer modeling of phase transformation from work-hardened austenite. *Iron and Steel Institute of Japan International*. 1992;32(3): 306-315.
- [5] Pandi R, Militzer M, Hawbolt EB, Meadowcroft TR. Effect of cooling and deformation on the austenite decomposition kinetics. In: *37th Mechanical Working and Steel Processing Conference Proceedings*. 1996. p.635-647.
- [6] Hanlon DN, Sietsma J, Zwaag S. The effect of plastic deformation of austenite on the kinetics of subsequent ferrite formation. *Iron and Steel Institute of Japan International*. 2001;41(9): 1028-1036.
- [7] Lan YJ, Xiao NM, Li DZ, Li YY. Mesoscale simulation of deformed austenite decomposition into ferrite by coupling a cellular automaton method with a crystal plasticity finite element model. *Acta Materialia*. 2005;53(4): 991-1003.
- [8] Yamanaka A, Takaki T, Tomita Y. Simulation of austenite-to-ferrite transformation in deformed austenite by crystal plasticity finite element method and multiphase-field method. *Iron and Steel Institute of Japan International*. 2012;52(4): 659-668.
- [9] Karpov VG. Nucleation in disordered media. *Physical Review B*. 1994;50(13): 9124-9127.
- [10] Karpov VG, Oxtoby DW. Nucleation in disordered systems. *Physical Review B*. 1996;54(14): 9734-9745.
- [11] Zisman AA, Rybin VV. Mesoscopic stress field arising from the grain interaction in plastically deformed polycrystals. *Acta Materialia*. 1998;46(2): 457-464.
- [12] Ghosh C, Aranas C, Jonas JJ. Dynamic transformation of deformed austenite at temperatures above the Ae3. *Progress in Materials Science*. 2016;82: 151-233.
- [13] *Thermo-Calc Software*. Available from: <http://www.thermocalc.com> [Accessed 14th October 2020].
- [14] Vasilyev A, Sokolov D, Kolbasnikov N, Sokolov S. Modeling of the $\gamma \rightarrow \alpha$ transformation in steels. *Physics of the Solid State*. 2012;54(8): 1669-1680.
- [15] Zurob HS, Hutchison CR, Brechet Y, Purdy G. Modelling recrystallization of microalloyed austenite: effect of coupling recovery, precipitation and recrystallization. *Acta Materialia*. 2002;50(12): 3075-3092.
- [16] Verdier M, Brechet Y, Guyot P. Recovery of AlMg alloys: flow stress and strain-hardening properties. *Acta Materialia*. 1999;47(1): 127-134.
- [17] Vasilyev A, Rudskoy A, Kolbasnikov N, Sokolov S, Sokolov D. Physical and mathematical modeling of austenite microstructure evolution processes developing in line-pipe steels under hot rolling. *Material Science Forum*. 2012;706-709: 2836-2841.
- [18] Vasilyev AA, Sokolov SF, Kolbasnikov NG, Sokolov DF. Effect of alloying on the self-diffusion activation energy in γ -iron. *Physics of the Solid State*. 2011;53(11): 2194-2200.
- [19] Liubov BY. *Kinetics of Phase Transformations*. Moscow: Metallurgy; 1969. (In Russian)

- [20] Vasilyev AA, Golikov PA. *Models for Calculating Carbon Diffusion Coefficient in Steels and Examples of their Practical Use*. St. Petersburg: POLYTECH-PRESS; 2019. (In Russian)
- [21] Saito Y, Shiga C. Computer simulation of microstructural evolution in thermomechanical processing of steel plates. *Iron and Steel Institute of Japan International*. 1992;32(3): 414-422.
- [22] Vasilyev A, Sokolov D, Sokolov S, Kolbasnikov N. Integral computer model for simulating microstructure evolution during thermomechanical processing and heat treatment of steels and predicting their final mechanical properties. To be published in *Material Science Forum*. [Preprint] 2020.